

Impact of Structural Dimensions and Poles on the Torque Performance of Dual-stator Permanent Magnet Machines

C. C. Awah¹, O. I. Okoro¹, I. E. Nkan², E. E. Okpo²



¹Department of Electrical and Electronic Engineering, Michael Okpara University of Agriculture, Umudike, Nigeria

²Department of Electrical and Electronic Engineering, Akwa Ibom State University, Mkpato Enin, Nigeria

ABSTRACT: The impact of structural dimensions and rotor pole numbers on the load and no-load torques of dual stator permanent magnet machine is investigated and presented in this work. Finite element analysis (FEA) is adopted in the prediction, since it exhibits higher computation accuracy compared to other methods such as analytical modelling and techniques, etc. Version 15.0 of MAXWELL/ANSYS-2D software is implemented in the entire computations. The considered structural dimensions include: rotor centrifugal size (R_{th}), aspect ratio (S_r), permanent magnet width (M_{th}), outer stator tooth width (T_{th}), rotor outer pole arc/pitch ratio (γ_1) and rotor inner pole arc/pitch ratio (γ_2). Also, model topologies having stator pole (S) and rotor pole (P) numbers i.e. 6S/10P, 6S/11P, 6S/13P and 6S/14P, are compared. The results show that the shaft torque and no-load torque would reasonably depend on the adopted machine's structural dimensions; in addition to the impact of rotor pole number. More so, it is observed that the optimal output torque of a given machine may not necessarily occur at the same operating structural point with that of the required least no-load torque. Implementation of the optimum structural dimensions would result to largest average output electromagnetic torque from the machine. Moreover, practically all the most optimum results are obtained from the 6S/11P machine type. The useable average shaft torque from the simulated models is approximately: 2.33 Nm, 4.16 Nm, 3.75 Nm and 2.31 Nm, for the 6S/10P, 6S/11P, 6S/13P and 6S/14P categories, respectively. Similarly, least values of the no-load torque in the compared machine types are 1.2 Nm, 0.08 Nm, 0.04 Nm and 0.68 Nm i.e. for the 6S/10P, 6S/11P, 6S/13P and 6S/14P machine topologies.

KEYWORDS: Dual stator, No-load torque, Permanent magnet machine, Pole number, Shaft torque, Structural dimensions.

[Received Nov. 15, 2021; Revised Feb. 13, 2022; Accepted Mar. 15, 2022]

Print ISSN: 0189-9546 | Online ISSN: 2437-2110

I. INTRODUCTION

Geometric structural dimensions and number of rotor poles are vital in the electromagnetic performance of any given electrical machine because, machine performance metrics would greatly depend on the optimal structural values of the machine while the pole numbers would in addition to other factors influence the machine's operating frequency and rotational speed, Xu *et al.*, (2021). Since, the effect of the aforementioned parameters cannot be underestimated; thus, the impact of structural parameters as well as the effect of rotor pole numbers on shaft torque and no-load (cogging) torque of a new kind of dual stator permanent magnet machine is precisely studied in this present work.

The impact of machine's structural plan such as its slot opening size, permanent magnet width and volume on its output performance is proved to be large in permanent magnet (PM) machines, as demonstrated in Wang *et al.*, (2019). Lots of research about the influence of key design parameters on the output of different double stator permanent magnet machine topologies have been conducted and many more are still underway, owing to the significant impact of these parameters on the overall machine productivity, as evidenced in Awah and Zhu (2016); Awah and Okoro (2021).

Further, influence of rotor pole number on the electromagnetic performance of both double stator (DS) and single stator (SS) permanent magnet (PM) machines presented in Awah and Okoro (2019) and Zheng *et al.*, (2019), reveal that PM machines having odd number of rotor poles usually have better output performance than their equivalents that have even number of rotor poles. More so, the machines that have even number of rotor poles are usually characterized with high harmonic components and consequently, larger amount of no-load (cogging) torque despite its attendant torque ripple/pulsation effects, Zhao *et al.*, (2020).

It is reported in Li *et al.*, (2012) that geometric structural dimensions of single stator flux-switching permanent magnet machine, in particular, its aspect ratio would greatly affect the machine's overall performance; the selected aspect ratio should be done through adequate optimization technique, in order to produce the best output torque capacity. Nevertheless, the adopted analytical method in Li *et al.*, (2012) is less accurate than the finite element approach undertaken in this current study. Further, significant impact of electric machine's aspect ratio on the electromagnetic output of multi-phase flux-switching machine is reiterated and proved in Li *et al.*, (2015) with test results. Moreover, rotor and stator pole permutations

*Corresponding author: ccawah@ieee.org

doi: <http://dx.doi.org/10.4314/njtd.v19i1.8>

are also proven to influence loss magnitude as well as efficiency of the machine. Therefore, optimal structural dimensions plus right stator and rotor pole selections are essential in any electrical machine design for complete machine effectiveness. Electrical machine effectiveness includes the machine's electromagnetic torque and power outputs, as well as low effects of undesirable qualities such as unbalanced magnetic force, no-load/cogging torque, torque ripple, total harmonic distortion and vibration, etc. Thus, Lu *et al.*, (2021) proved that appropriate combination of rotor pole number and stator tooth number in a permanent magnet electric machine could significantly reduce the force and vibration effects in such machine.

The investigated machine in this present study is a classical flux-switching permanent magnet (FSPM) machine and it usually has saliency ratio of 1, because it exhibits similar axes inductance. As a result, the reluctance torque component of FSPM machines is negligible compared to the ones of traditional PM machines. Meanwhile, significant portion of the generated torque in FSPM machine is contributed predominantly by the PM torque component. In contrast, the output torque production of conventional permanent magnet machines is dependent on the difference and ratio of its axes inductance i.e. inductance in the direct-axis and quadrature-axis directions, as observed in Vahaj *et al.*, (2019). Effect of these axes inductance in addition to rotor geometric design on the output torque of an electric machine is established to be reasonably high in Raj and Kavitha (2017). As a result, adequate geometric plan and high winding inductances are recommended for paramount machine performance, besides the inherent pole number effect.

Similarly, the investigation of flux-reversal permanent magnet machine presented in Xie *et al.*, (2019) show that rotor and stator pole combinations, in addition to other leading geometric dimensions of electric machines are important in deciding the machine's output performance. More so, it is noticed that there is an inverse correlation between the no-load torque and average electromagnetic torque of an electric machine; while the trend of torque ripple and no-load torque is in harmony with each other. However, it is proved in Li *et al.*, (2018) that the amount of torque ripple in an electrical machine is a direct consequence of its overload capacity combined with its stator structural design and winding arrangement. Therefore, in electrical machine design, a concession is usually made between the developed electromagnetic torque and the associated torque ripple degree of the given machine.

The size of slot opening as well as the machine's stack size would have great influence on the performance of a given permanent magnet (PM) machine, as established in Li *et al.*, (2018) with experimental facts; the larger the parameters, then, the higher its output performance; though, the performance will also be constrained by the overall machine outer diameter. Also, both the shape of the generated electromotive force and amplitude of the resulting electromagnetic torque could be influenced by the machine's geometrical structural size and dimensions, as noted in Zhou

et al., (2019). Although, quick analytical methods could be used to estimate both the basic dimensions and performances of a given permanent magnet machine compared to time-consuming finite element analysis (FEA), as claimed in Zhou *et al.*, (2019). In actual fact, the superiority of FEA over analytical method is overwhelming in terms of higher result accuracy.

Analytical expressions that relate the size of different kinds of electric machine with its output torque is detailed in Lipo *et al.*, (2020); special reference is made to the relationship between generated flux density in the airgap and slot opening width for a fixed current concentration level. Again, these analytical expressions are only but mathematical approximations which lack some level of prediction exactness. The adopted finite element numerical approach in this current study seems to be the most accurate technique; the correctness of this method is emphasized in Wang *et al.*, (2019). It is worth mentioning, that flux-switching PM machines specifically are characterized with possible magnet demagnetization and high flux leakage defects, despite its enviable torque production prowess. Further, Zhu *et al.*, (2021) proved that structural/geometric values coupled with stator and rotor pole arrangements of a given permanent magnet machine, would influence its electromagnetic output to a great extent. Thus, adequate care should be given to the structural values as well as the rotor/stator pole plan of the machine in order to achieve the optimal electromagnetic performance or results from the device/system.

Precisely, the effect of basic structural geometric dimensions on both shaft torque and no-load torque of a new kind of dual stator permanent magnet machine is investigated and reported in this present study, in order to have better understanding about the use of optimal machine structural values and suitable rotor pole number and stator tooth number combinations, for improved machine output performance.

II. MATERIALS AND METHODS

Finite element analysis (FEA) is used in calculating the results, due to its higher level of correctness compared to other methods such as the analytical and mathematical modelling techniques. The analytical methods are saddled with vast assumptions, as shown in Ni *et al.*, (2020) and Zhang *et al.*, (2020). Moreover, the consequences of these assumptions lead to reasonable inconsistency between FEA and analytically estimated results, as demonstrated in Vahaj *et al.*, (2019). The analyzed model structure with its corresponding dimensions is displayed in Figure 1. B_{th} represents the outer stator back-iron thickness.

Shaft torque and no-load torque of the investigated machine topologies having different number of rotor poles are considered in this study. It is worth noting that the investigated machine models were first subjected to a global optimization process during its initial design phase, where all the structural parameters of the models are optimally realized simultaneously using in-built algorithm of the implemented software. Note that the conducted global optimization has one goal, which is to obtain largest output torque from the model;

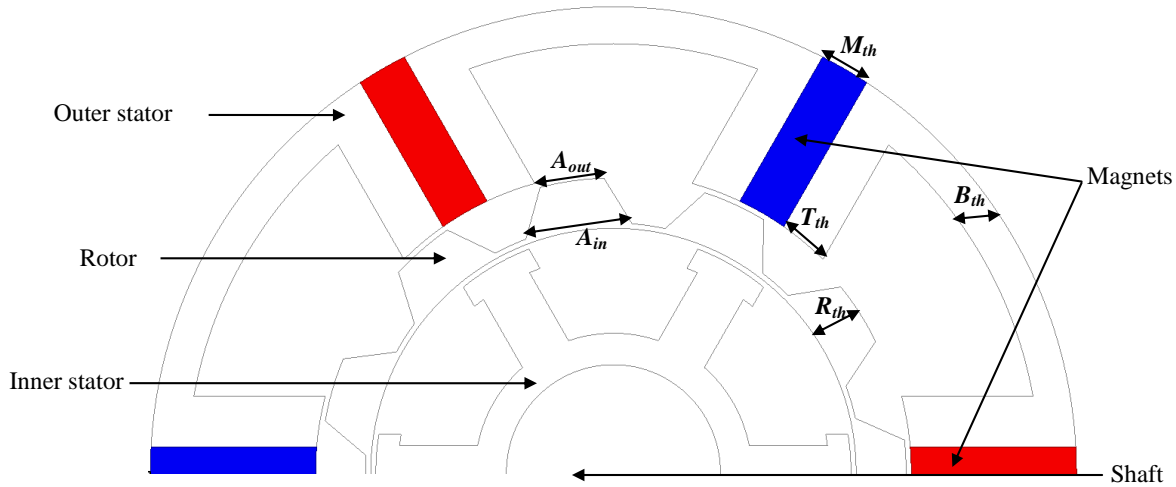


Figure 1: The developed machine half-structure.

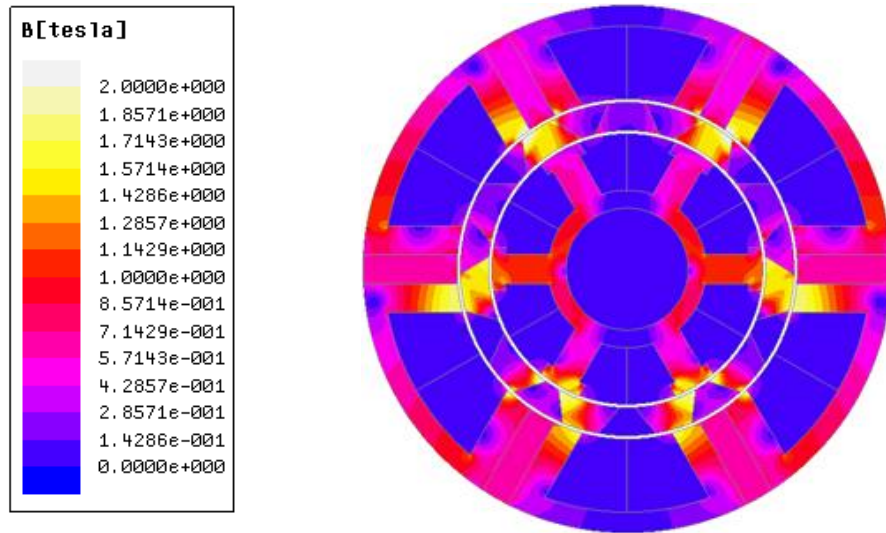


Figure 2: Flux density outline on no-load.

however, without considering the impact of no-load/cogging torque on open circuit condition. Also, magnetic flux density FEA diagram of the analyzed machine is shown in Figure 2. It is observed that the rotor and stator teeth have high capacity to be overloaded, owing to the enormous energy conversion processes that happen around these regions which are adjacent to the machine's air-gap. The core parts are made of steel material while the magnets are made of neodymium-iron-boron rare-earth magnetic material. Overall size of the machine is 90 mm while its airgap size is 0.5 mm. It has an active length of 25 mm. The operating speed of the models is 400 r/min. Also, the analysed model is a three-phase device having 72 turns per phase. Note that the studied machine is a flux-switching permanent magnet (FSPM) machine, though with double stator structure. The predicted aspect ratio of the investigated machine types is estimated using Eqn. (1).

$$S_r = \frac{\text{Rotor airgap diameter}}{\text{Overall stator diameter}} \quad (1)$$

Similarly, the rotor outer pole arc/pitch ratio (γ_1), and rotor inner pole arc/pitch ratio (γ_2), are calculated using Eqns. (2) and (3) respectively.

$$\gamma_1 = \frac{A_{out}}{\text{rotor pole pitch}} \quad (2)$$

$$\gamma_2 = \frac{A_{in}}{\text{rotor pole pitch}} \quad (3)$$

Moreover, the expression of the predicted no-load torque, T_{load} is given in Eqn. (4).

$$T_{nload} = \sum_{n=1}^{\infty} T_n \sin(nL_{cm}\theta + \theta_n) \quad (4)$$

where T_n and θ_n are the magnitude and phase of n^{th} harmonic order respectively, L_{cm} is the lowest common multiple between the rotor pole and stator tooth numbers (Husain *et al*, 2019).

More so, the initial rotor position, P_{ir} , which is associated with direct-axis of the machine is at 90 degrees shift with the machine's quadrature-axis position; thus,

$$P_{ir} = 90^\circ / P \quad (5)$$

where P is the rotor pole number.

It is worth noting that a time-stepping transient magnetic solver is used to estimate the torques, since this approach would produce the most outstanding result, as stated in Maxwell-2D User's guide. The adopted transient solver calculates the electric and magnetic fields effectively around the airgap, as functions of rotor angular position and time with the help of a band section which wraps all the moving parts in one envelop. Since the torque, especially the no-load torque is very sensitive to the employed mesh elements, the adopted mesh elements are based on element-length refinement, to ensure higher accuracy of the obtained results. These lengths are listed below:

Airgap and band region

Maximum length of element: 0.5 mm

Rotor and stator core sections

Maximum length of element: 1 mm

Permanent magnet and slot areas

Maximum length of element: 1 mm

It is worth mentioning that the adopted software automatically generates the simulation results of the model in Figure 1. The computer-generated results are produced as numerical data in tabular form over one electric period, after which the results are then post-processed further for ease of interpretation. The machine structural parameters are subjected to parametric optimization over different geometric range, at fixed copper loss condition to obtain the optimal average torque and required minimum no-load/cogging torque.

III. RESULTS AND DISCUSSION

A) Influence of Geometric Dimensions and Rotor Pole Number on Shaft Torque and No-Load Torque

Structural dimensions are very vital in defining the overall electromagnetic performance of any given electrical machine. This section evaluates the impact of these structural dimensions on both on load torque and no-load torque of the developed dual stator permanent magnet machine having varying number of rotor poles. Figure 3 shows the influence of rotor centrifugal size (R_{th}) and aspect ratio (S_r) on shaft torque. It could be seen that the 6S/11P machine type has the best shaft torque while the optimum centrifugal size of the

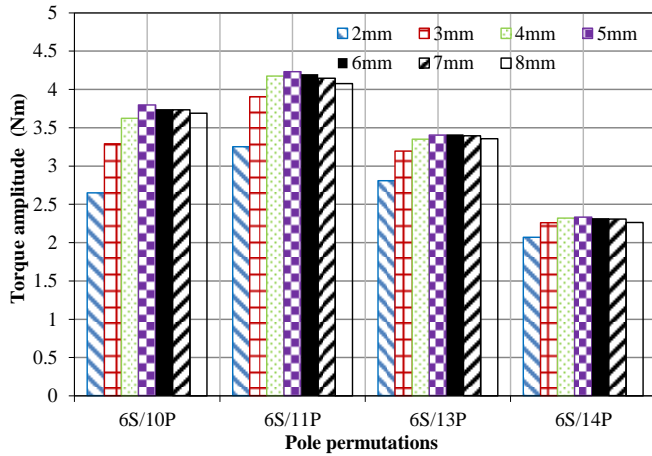
rotor to realize the largest shaft torque is 5 mm, in the compared machine types. More so, the least of the produced shaft torque is being contributed by the machine that has 14 rotor pole number and 6 stator slots i.e. 6S/14P, undertaken at constant copper loss of 30 Watts. Further, effect of the machine's aspect ratio on shaft torque is depicted in Figure 3(b). The varying aspect ratios produced different amplitudes of shaft torque. The optimum aspect ratio occurred at a value of 0.7 in the 6S/11P machine type; also, the 6S/11P takes the lead in terms of shaft torque amplitude. Meanwhile, the optimum value of the aspect ratio is: 0.75, 0.65 and 0.65 for the 6S/10P, 6S/13P and 6S/14P machine configurations, respectively.

Similarly, the impact of permanent magnet width (M_{th}) on shaft torque is displayed in Figure 4(a). It is observed that optimal magnet width is obtained in the 6S/11P topology at a value of 5 mm, while its corresponding peak value that yields ideal shaft torque in the 6S/10P, 6S/13P and 6S/14P machine types is: 5mm, 6 mm and 6mm, respectively. More so, the effect of outer stator tooth width (T_{th}) on shaft torque is depicted in Figure 4(b). The largest shaft torque is obtained in the 6S/10P machine type at T_{th} value of 3 mm, with equivalent optimum value of 4mm, 5mm and 4mm in the 6S/11P, 6S/13P and 6S/14P machine topologies. Although the peak-to-peak values of shaft torque is large in the 6S/10P machine topology on varying the outer stator tooth width (T_{th}); however, the predicted average torque values in all the analyzed machine types show that the machine topology having 11-pole i.e. 6S/11P exhibits the largest average torque, as shown in Table 1.

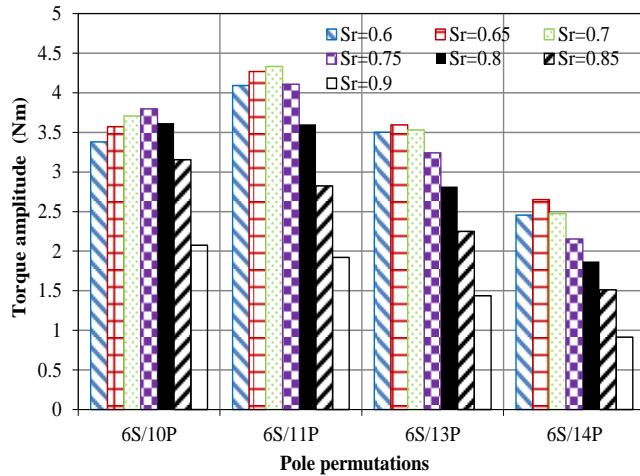
The 6S/13P is next to 6S/11P machine configuration, in terms of average torque magnitude. Zheng *et al* (2019) proved that FSPM machines having even number of rotor poles usually have higher pulsation effect than its counterparts that have odd number of rotor poles, owing to large disparity in the harmonic contents of the two groups of machine. These harmonic elements tend to be higher in the machines that have even number of rotor poles. The recorded maximum shaft torque in the 6S/10P machine type is as a result of high torque ripple/pulsation effect of the considered 10-pole machine, which is a resulting effect of its high harmonic worth.

Table 1: Average torque at varying outer stator tooth width.

Outer stator tooth width (T_{th}), mm	6S/10P	6S/11P	6S/13P	6S/14P
2	1.60	2.56	2.26	1.39
3	2.03	3.48	2.94	1.75
4	2.21	4.01	3.30	1.90
5	2.22	4.10	3.35	1.89
6	2.10	3.85	3.17	1.76
7	1.93	3.48	2.88	1.59
8	1.76	3.11	2.58	1.42

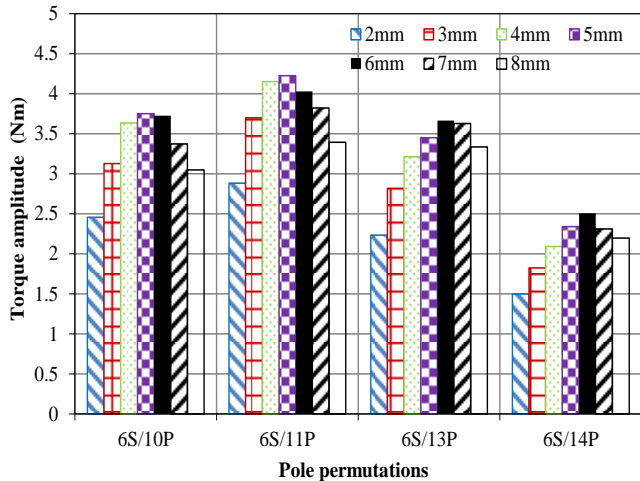


(a) Rotor centrifugal size (R_{th}).

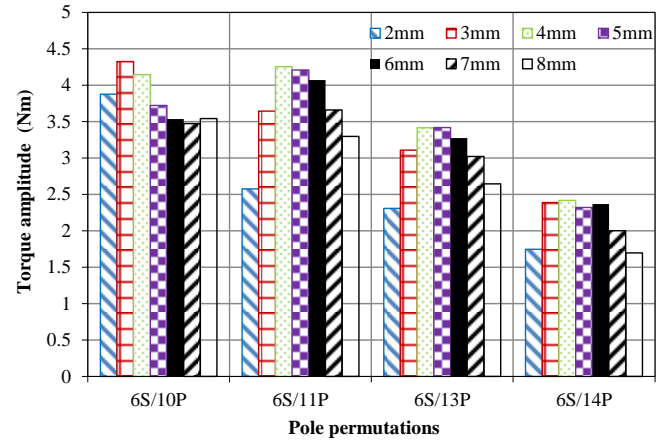


(b) Aspect ratio (S_r).

Figure 3: Effect of rotor centrifugal size (R_{th}) and aspect ratio (S_r) on shaft torque.



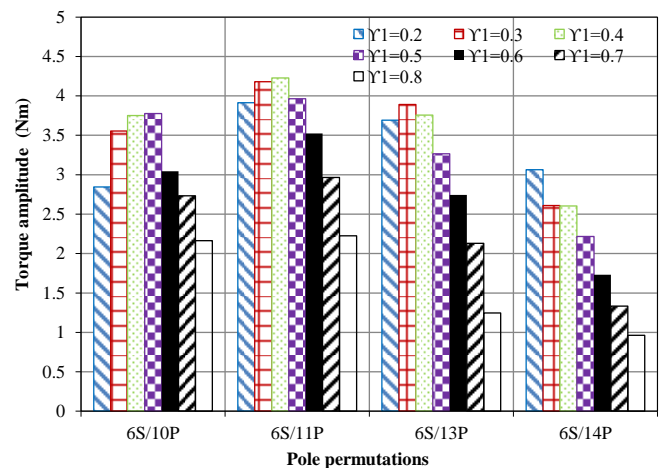
(a) Permanent magnet width (M_{th}).



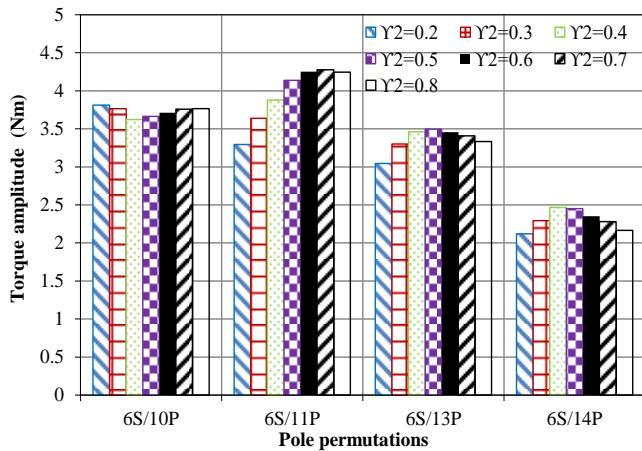
(b) Outer stator tooth width (T_{th})

Figure 4: Effect of permanent magnet width (M_{th}) and outer stator tooth width (T_{th}) on shaft torque.

Furthermore, the effects of rotor outer pole arc/pitch ratio (γ_1) and rotor inner pole arc/pitch ratio (γ_2) are presented in Figure (5). These effects would be dependent on the amount of linking fluxes on the rotor tips of the investigated machine, which would also be a function of the rotor angular positions and hence, the time of operation. The linking fluxes are often deposited mostly on these pole arcs due to the huge permeability content of the selected steel core material plus its nearness to the airgap area, where high level electromagnetic energy conversion process takes place. The respective best values for the γ_1 and γ_2 are 0.4 and 0.7 in the 6S/11P machine configuration. In both cases, the worst scenarios of the produced shaft torque are attained in the 6S/14P machine type. Moreover, the optimum value of γ_1 in the 6S/10P, 6S/13P and 6S/14P is 0.5, 0.3 and 0.2, respectively; their corresponding optimum γ_2 value is: 0.2, 0.5 and 0.4. It is worth noting that the optimal values of γ_1 in the machine topologies vary inversely proportionally to the produced shaft torques.



(a) Rotor outer pole arc/pitch ratio (γ_1).

(b) Rotor inner pole arc / pitch ratio (γ_2).**Figure 5: Effect of rotor outer pole arc/pitch ratio and rotor inner pole arc/pitch ratio on shaft torque.**

Generally, the resulting value of shaft torque under each specific varying structural dimension would depend upon the available space for the armature conductors owing to these variations and consequently, upon the applied phase currents due to these conditions. In most case scenarios shown in Figures 3-5, the ensuing shaft torque magnitude due to the changing structural dimensions would rise in the first instance, and then, decrease in value owing to the amount of the generated magnetic flux under each specified operating condition.

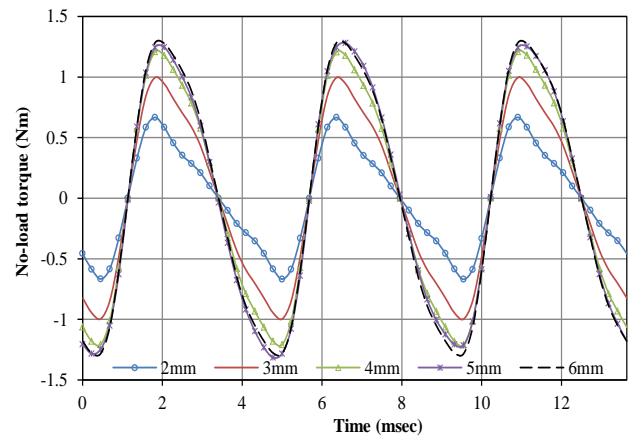
The no-load torque of the analyzed machine configurations having 10-pole, 11-pole, 13-pole and 14-pole i.e. 6S/10P, 6S/11P, 6S/13P and 6S/14P are displayed in Figures 6-11. It is worth mentioning that low no-load (cogging) torque amplitude is inherently possible in FSPM machines having odd number of rotor poles, as proved in Zhao *et al*, (2020) and reconfirmed in Figures 6–11 of the present investigation. Furthermore, the rotor centrifugal size (R_{th}) waveform variations with no-load torque of the compared machine types are depicted in Figure 6. It is shown that the minimum amount of no-load torque is obtained in the 6S/13P machine type while the largest amount of no-load is recorded in the 6S/10P.

However, the no-load torque sensitivity to the machine's rotor centrifugal size is apparently insignificant in the 6S/11P and 6S/14P relative to the 6S/10P machine type, as shown in Figure 6. More so, the predicted no-load torque in the compared machine types except the 6S/10P machine is relatively low compared to their respective produced shaft torque. It should be noted that the sensitivity effect of aspect ratio on no-load torque in the analyzed machine models is noticeable as shown in Figure 7, owing to the significant impact of aspect ratio on the overall performance of electrical machines, as reported in (Li *et al*, 2015).

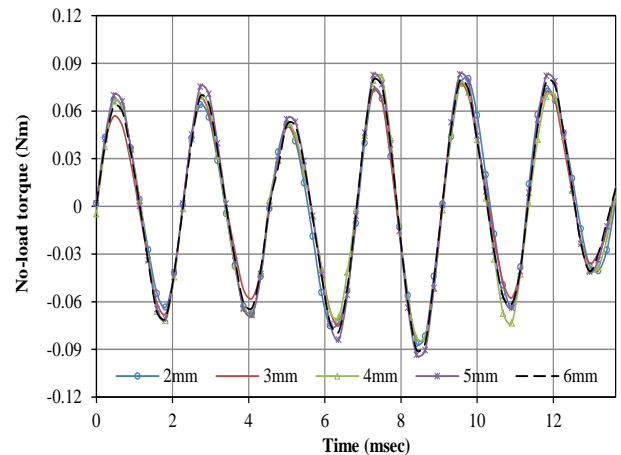
Note that the no-load torque waveform is symmetrically distributed over the simulation time. It is important to note that high amount of no-load torque is unfavorable to the

machine's output torque and overall performance quality. In all cases, the number of no-load torque rotations (cyclic order) in the machine types having even number of rotor poles is one-half of its equivalent odd number of rotor poles, as seen in Figures 6-11. This cyclic order phenomenon is because number of no-load torque rotations is dependent upon the machine's pitch ratio and lowest common factor (*LCF*) between stator and rotor pole numbers of each machine type, as detailed in Zhao *et al* (2020).

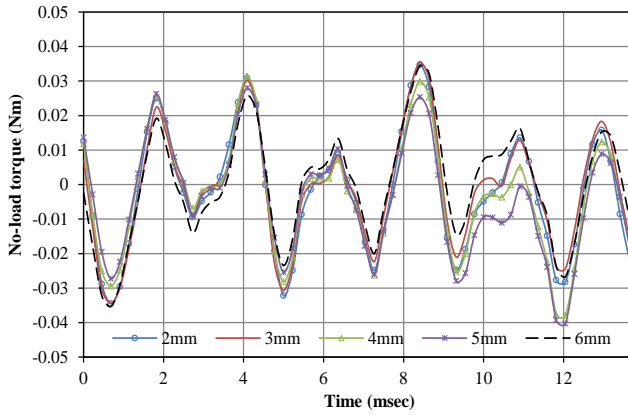
Further, it could be inferred from (Awah and Okoro, 2019) that the ratio of the machine's pitch ratio to *LCF* is similar among the different sets of machine topologies. For example, 6S/10P and 6S/14P would have 3 each as a ratio, while 6S/11P and 6S/13P would have 6 each. These ratios correspond to the number of no-load torque rotations in the analyzed machine types per electric period.



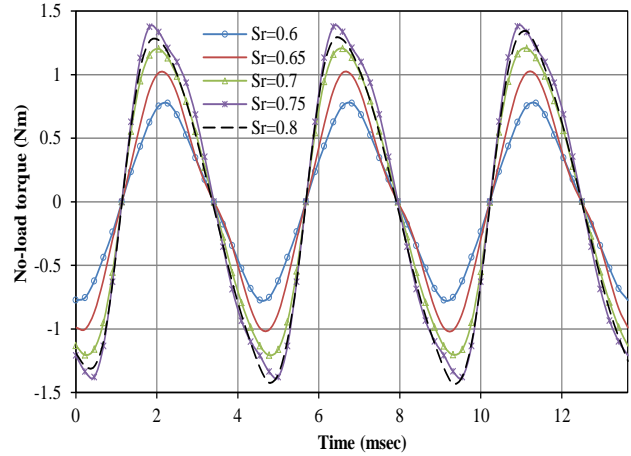
(a) No-load torque versus time, 6S/10P.



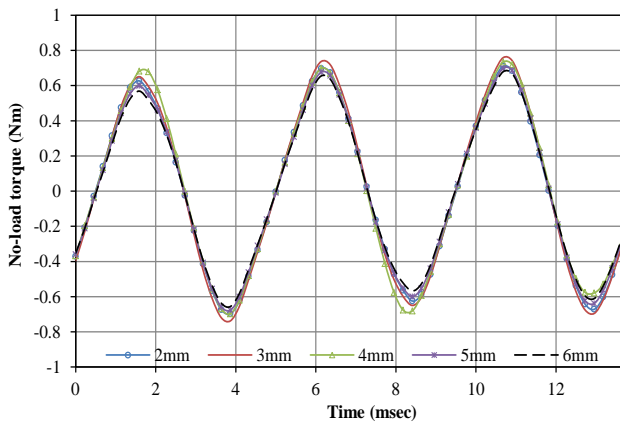
(b) No-load torque versus time, 6S/11P.



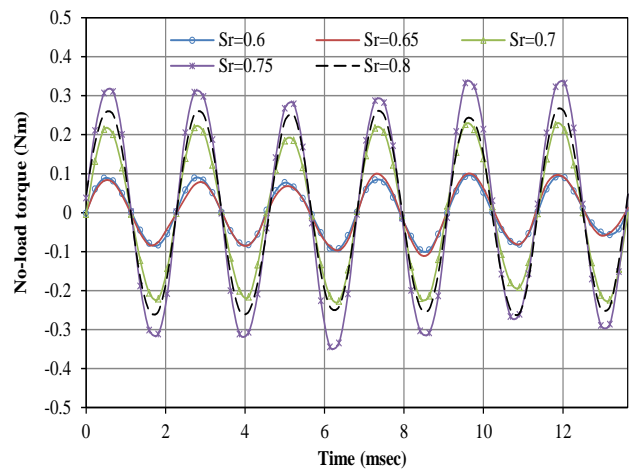
(c) No-load torque versus time, 6S/13P.



(a) No-load torque versus time, 6S/10P.



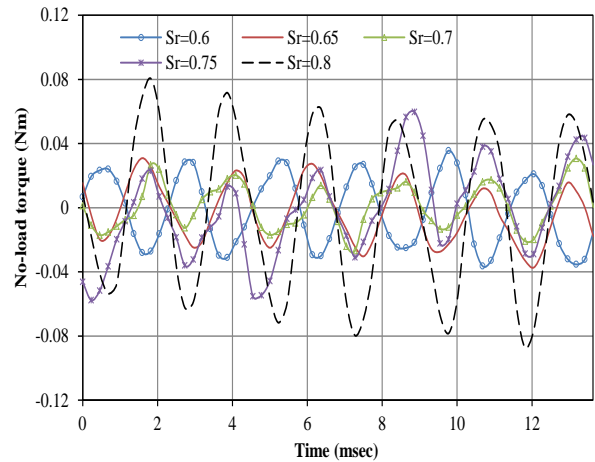
(d) No-load torque versus time, 6S/14P.



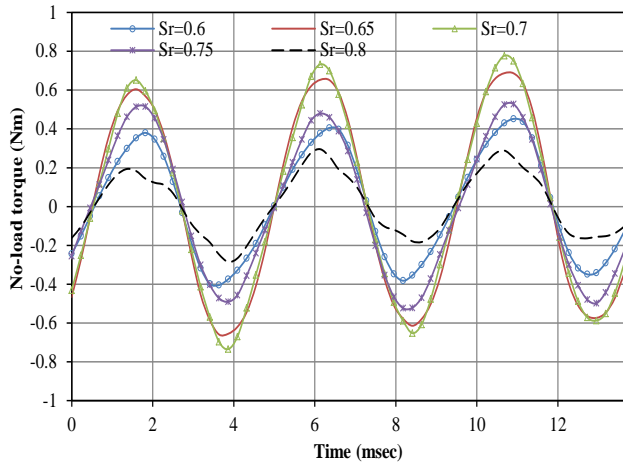
(b) No-load torque versus time, 6S/11P.

Figure 6: Effect of rotor centrifugal size (R_n), on open-circuit condition.

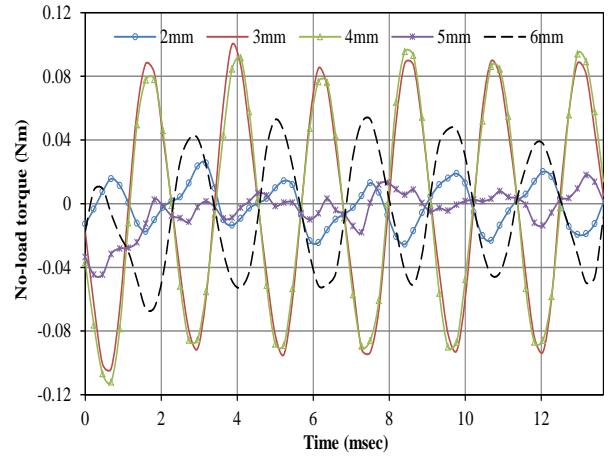
In order to obtain the largest output torque from the machine, then, minimum amount of no-load torque is recommended. Thus, minimum values of the no-load torque would occur at the rotor centrifugal size of 2 mm, 3 mm, 5 mm and 6 mm, respectively for the 6S/10P, 6S/11P, 6S/13P and 6S/14P machine types. The trend shows a direct/linear proportionality between the rotor centrifugal size and the machine's increasing rotor pole numbers. Similarly, the respective least amount of no-load torque would occur when S_r values are 0.6, 0.6, 0.75 and 0.8 for the 6S/10P, 6S/11P, 6S/13P and 6S/14P machine categories. Meanwhile, the recorded largest amount of no-load torque in the different machine types occurred at S_r value of 0.75, 0.75, 0.8 and 0.7 i.e. for the 6S/10P, 6S/11P, 6S/13P and 6S/14P machine, respectively. However, note that collective effect of the other machine structural values is indispensable to the overall electromagnetic output of the system at each operating condition.



(c) No-load torque versus time, 6S/13P.

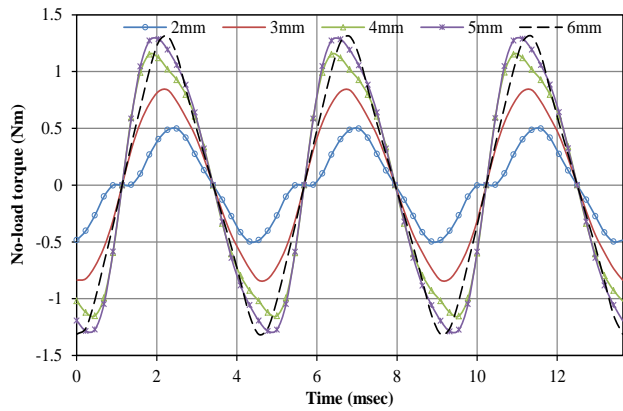


(d) No-load torque versus time, 6S/14P.

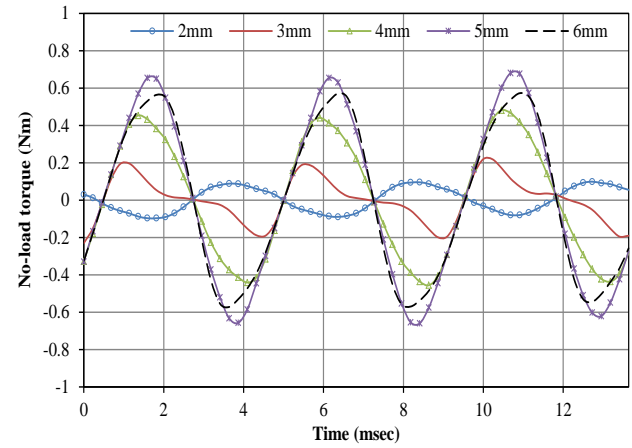


(c) No-load torque versus time, 6S/13P.

Figure 7: Effect of aspect ratio (S_r), on open-circuit condition.

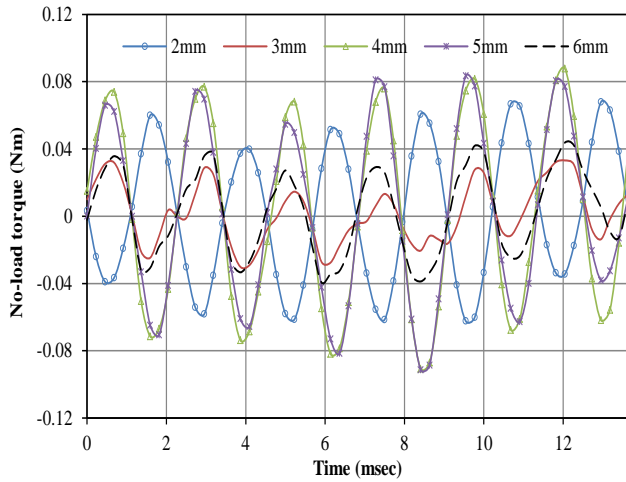


(a) No-load torque versus time, 6S/10P.

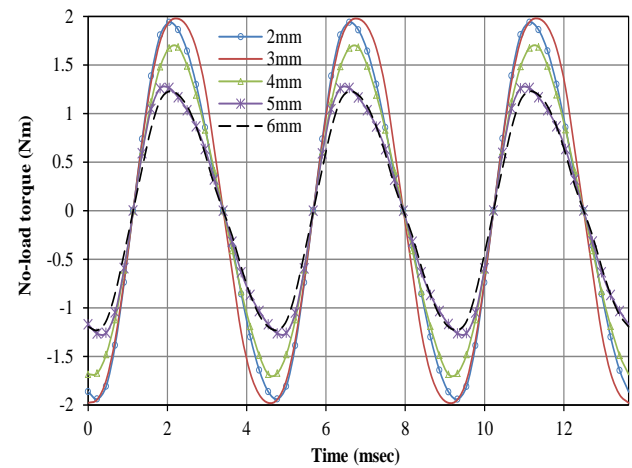


(d) No-load torque versus time, 6S/14P.

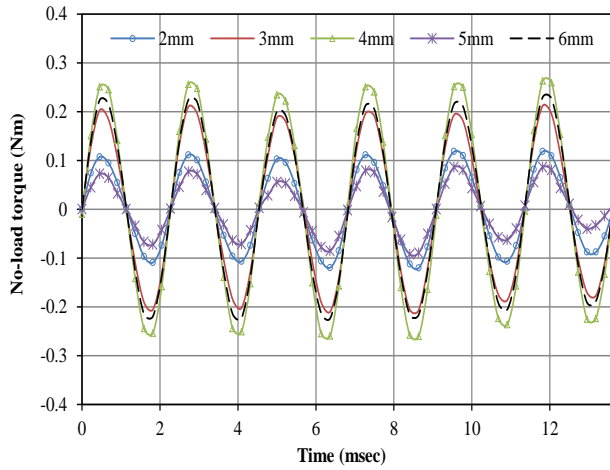
Figure 8: Effect of permanent magnet width (M_{th}), on open-circuit condition.



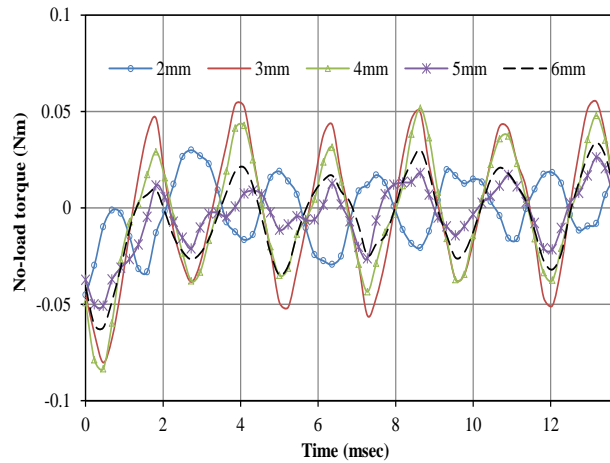
(b) No-load torque versus time, 6S/11P.



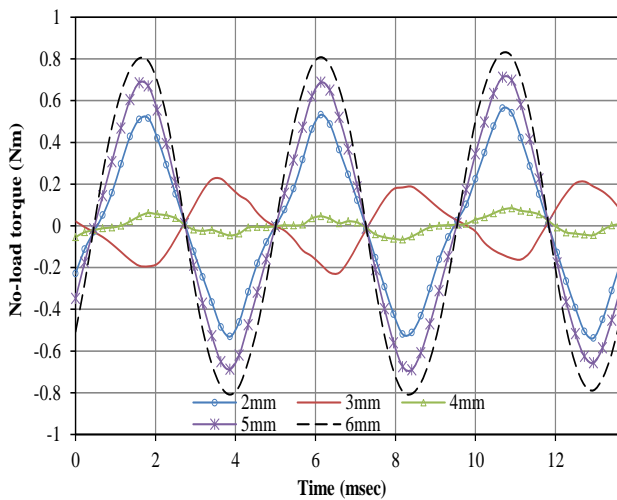
(a) No-load torque versus time, 6S/10P.



(b) No-load torque versus time, 6S/11P.



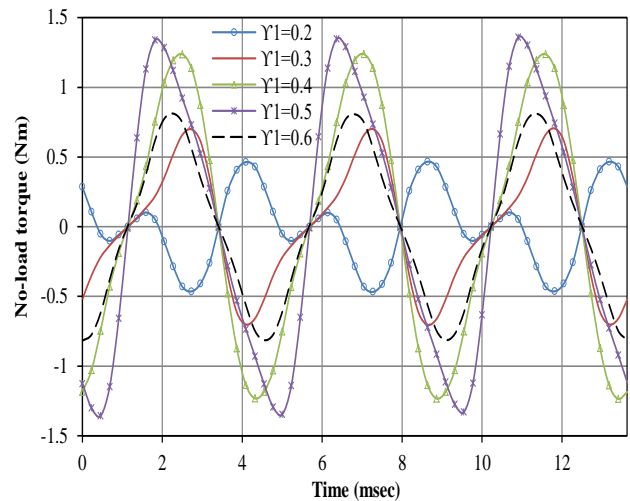
(c) No-load torque versus time, 6S/13P.



(d) No-load torque versus time, 6S/14P.

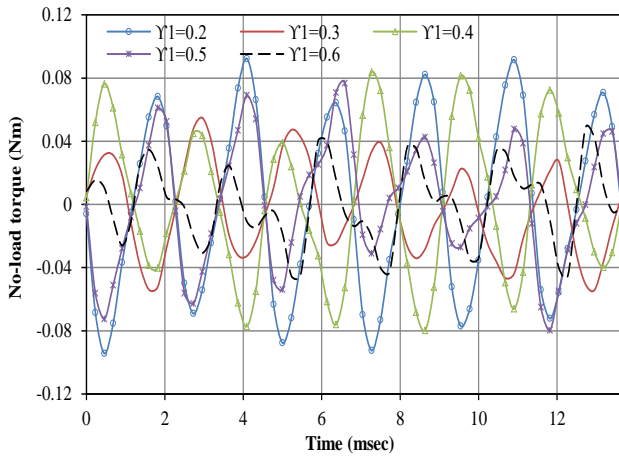
Also, it is obvious from Figures 7(c), 8, 9(c), 10 and 11(c) that there could be angular phase shifts of the rotor as each of the geometric structural parameter varies over time. Also, the no-load torque waveforms show that there could be great difference in the shape and amplitude of the resulting waveforms, when considering the impact of a particular structural dimension. More so, the variation of no-load torque with permanent magnet width (M_{th}) is shown in Figure 8. The lowest amount of no-load torque would be obtained in the machine when M_{th} is: 2 mm, 3 mm, 5 mm and 2 mm, for the 6S/10P, 6S/11P, 6S/13P and 6S/14P machine types, respectively. Similarly, the corresponding minimum no-load torque value is obtainable at the T_{th} point of: 6 mm, 5 mm, 5 mm, and 4 mm, respectively, for a changing outer stator tooth width, as depicted in Figure 9.

Nevertheless, there could be a compromise between the magnitude of shaft torque and its corresponding influence on the no-load torque. An optimization target of a given electric machine could be chosen in order to have both large output torque and low no-load (cogging) torque by manipulating the relevant structural parameters, as established in Vahaj *et al*, (2019). However, a given flux-switching permanent magnet (FSPM) machine having low no-load torque i.e. low cogging torque would naturally have large output torque and vice-versa. Therefore, in order to obtain a higher average torque from an FSPM machine; the machine's structural dimensions could be designed and optimized with the aim(s) to achieve the lowest no-load torque/cogging torque while outputting the largest average torque via the shaft, from the considered model.

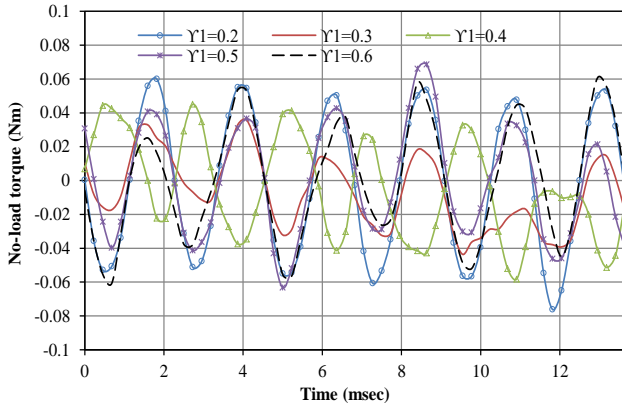


(a) No-load torque versus time, 6S/10P.

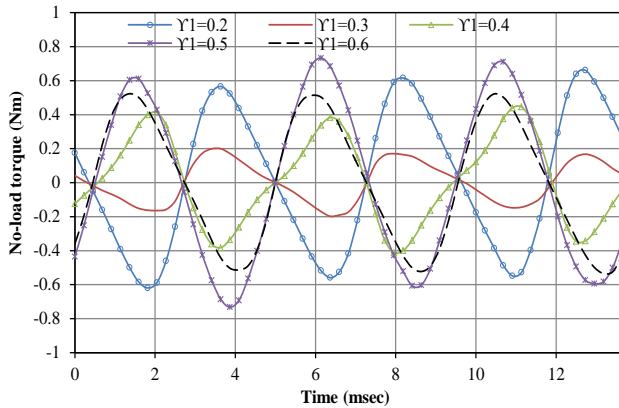
Figure 9: Effect of outer stator tooth width (T_{th}), on open-circuit condition.



(b) No-load torque versus time, 6S/11P.



(c) No-load torque versus time, 6S/13P.

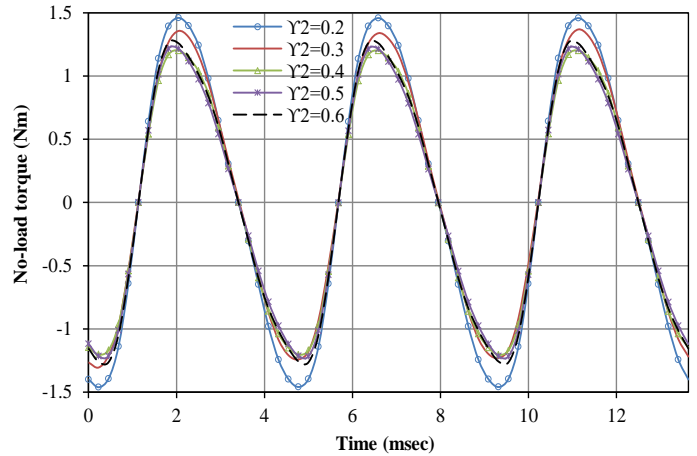


(d) No-load torque versus time, 6S/14P.

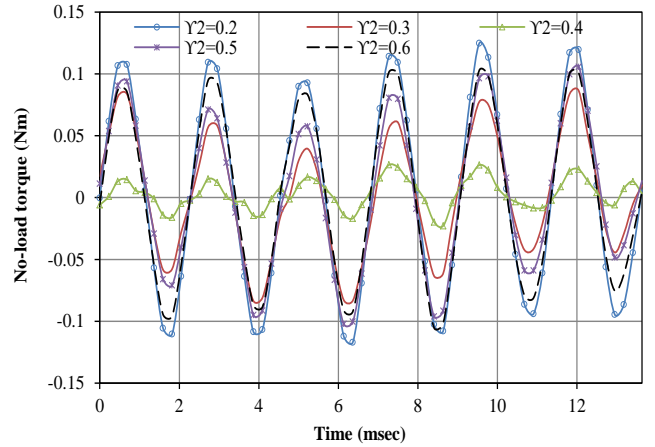
Figure 10: Effect of rotor outer pole arc/pitch ratio ($Y1$) on open-circuit condition.

Figures 10 and 11 show the variation of no-load torque with the rotor outer pole arc/pitch ratio ($Y1$) and rotor inner pole arc/pitch ratio ($Y2$), respectively. Again, it is shown that

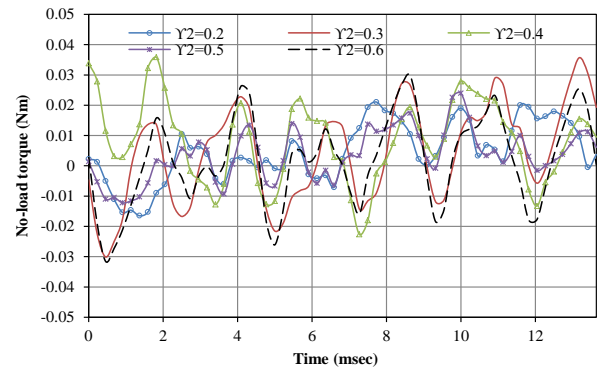
the machine types having even number of rotor poles possess higher no-load torque as $Y1$ and $Y2$ varies in one electric revolution. Although the predicted no-load torque waveform variations with $Y1$ and $Y2$ are uniformly distributed over time, they exhibit asymmetric outlines over the simulation time. The least no-load torque is realized when $Y1$ is: 0.2, 0.6, 0.3 and 0.3 for the 6S/10P, 6S/11P, 6S/13P and 6S/14P machine categories. Also, it has corresponding minimum no-load torque values at $Y2$ values of 0.4, 0.4, 0.2 and 0.2, respectively.



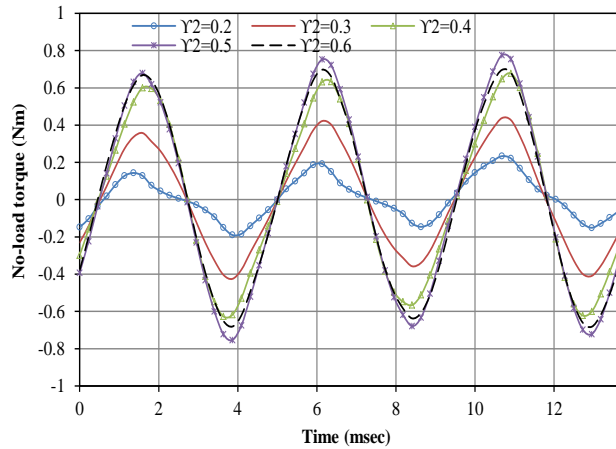
(a) No-load torque versus time, 6S/10P.



(b) No-load torque versus time, 6S/11P.



(c) No-load torque versus time, 6S/13P.



(d) No-load torque versus time, 6S/14P.

Figure 11: Effect of rotor inner pole arc/pitch ratio (γ_2) on open-circuit condition.

It is worth noting that the no-load or cogging torque in FSPM machine has negative influence on the resultant electromagnetic torque; meanwhile, the total output torque from such a machine is the algebraic sum of the no-load (cogging) torque and the on-load torque. Thus, the smaller the value of cogging torque, then, the larger the machine's total output torque, and vice-versa.

More importantly, since the various machine structural values affect the electromagnetic output of one another; then, it is paramount to conduct a multi-objective optimization with set goals as: largest average torque and least no-load torque, using a global optimization procedure. The global optimization scheme would ensure that all the machine structural dimensions are optimized concurrently at each specified time.

In general, it is worth stating that in all conditions, the structural machine geometric dimensions are inter-related with each other; thus, the best performance from a particular geometric dimension could jeopardize the output of the other and vice-versa. Also, the largest output torque of a given machine may not necessarily occur at the same operating structural point with that of the required least no-load torque. Therefore, it is recommended that a global optimization of all the structural dimensions concurrently with multi-objectives would yield the most competitive machine performance, since it offers higher flexibility for selecting the most appropriate structural dimensions. The finite element analysis (FEA) predicted numerical values of output torque from the shaft and no-load torque of the investigated machine types are enumerated in Table 2, under different working structural conditions.

Table 2: Torque values of the compared machine types at different structural dimensions.

Rotor centrifugal size (R_{th})	6S/10P	6S/11P	6S/13P	6S/14P
Maximum shaft torque, Nm	3.795	4.229	3.412	2.329
Average shaft torque, Nm	2.255	4.115	3.349	1.889
Maximum no-load torque, Nm	1.280	0.083	0.035	0.759
Aspect ratio (S_r)	6S/10P	6S/11P	6S/13P	6S/14P
Maximum shaft torque, Nm	3.794	4.332	3.594	2.650
Average shaft torque, Nm	2.336	4.127	3.522	2.087
Maximum no-load torque, Nm	1.379	0.333	0.081	0.777
Permanent magnet width (M_{th})	6S/10P	6S/11P	6S/13P	6S/14P
Maximum shaft torque, Nm	3.749	4.223	3.663	2.505
Average shaft torque, Nm	2.219	4.115	3.485	2.075
Maximum no-load torque, Nm	1.311	0.088	0.10	0.680
Outer stator tooth width (T_{th})	6S/10P	6S/11P	6S/13P	6S/14P
Maximum shaft torque, Nm	4.323	4.251	3.417	2.417
Average shaft torque, Nm	2.217	4.102	3.353	1.904
Maximum no-load torque, Nm	1.264	0.263	0.055	0.830
Rotor outer pole arc/pitch ratio (γ_1)	6S/10P	6S/11P	6S/13P	6S/14P
Maximum shaft torque, Nm	3.774	4.225	3.891	3.062
Average shaft torque, Nm	2.226	4.100	3.745	2.309
Maximum no-load torque, Nm	1.359	0.092	0.068	0.733
Rotor inner pole arc/pitch ratio (γ_2)	6S/10P	6S/11P	6S/13P	6S/14P
Maximum shaft torque, Nm	3.809	4.273	3.496	2.466
Average shaft torque, Nm	2.330	4.160	3.401	1.910
Maximum no-load torque, Nm	1.460	0.125	0.036	0.775

IV. CONCLUSION

The impact of machine structural dimensions of dual stator permanent magnet machine on shaft torque and no-load torque is presented. Two-dimensional finite element analysis (2D-FEA) technique is implemented in the entire calculations,

owing to its high level of prediction accuracy. The analysis reveal that each of the machine's structural dimensions at any particular instance, would affect both the magnitudes of shaft torque and no-load torque, as well as the angular phase shifts and shapes of the ensuing waveforms.

Moreover, the results show that the machines that have odd number of rotor poles exhibit desirable qualities such as smaller no-load torque and larger output torque from the shaft. More so, these structural dimensions are inter-related and dependent on each other; thus, could have a cumulative effect on the overall electromagnetic outcome of the machine, in the absence of multi-objective optimization aims and targets. Besides, machine type having 6S/11P has the most promising and optimum electromagnetic performance amongst all the compared machine topologies. Above all, it is concluded that the largest output torque of a given machine may not necessarily occur at the same operating structural point with that of the required least no-load torque; hence, multi-objective and global optimization is vital in a given electrical machine in order to realize the most promising optimal electromagnetic performance, from the considered machine.

REFERENCES

- Awah, C. C. and Okoro, O. I. (2019).** Fault-tolerant capability and torque-speed measurements of permanent magnet brushless AC machines. *Nigerian Journal of Technological Development*, 16 (4): 191–198.
- Awah, C. C. and Okoro, O. I. (2021).** Leading design parameters of dual-stator permanent magnet machine. *Bayero Journal of Engineering and Technology (BJET)*, 16 (2): 29–36.
- Awah, C. C. and Zhu, Z. Q. (2016).** Influence of rotor pole number on electromagnetic performance of double-stator switched flux PM machines. Paper presented at IEEE Vehicle Power and Propulsion Conference (VPPC), Hangzhou, China, 1–6, USA: IEEE.
- Husain, T.; I. Hasan; Y. Sozer; I. Husain and E. Muljadi. (2019).** Cogging torque minimization in transverse flux machines. *IEEE Transactions on Industry Applications*, 55 (1): 385–397.
- Li, D.; R. Qu; X. Zhang and Y. Liu. (2012).** Optimal split ratio in switched flux permanent magnet machines. Paper presented at IEEE Energy Conversion Congress and Exposition (ECCE), Raleigh, USA, 1925–1931, USA: IEEE.
- Li, D.; T. Zou; R. Qu and D. Jiang. (2018).** Analysis of fractional-slot concentrated winding PM vernier machines with regular open-slot stators. *IEEE Transactions on Industry Applications*, 54 (2): 1320–1330.
- Li, F.; W. Hua; M. Tong; G. Zhao and M. Cheng. (2015).** Nine-phase flux-switching permanent magnet brushless machine for low-speed and high-torque applications. *IEEE Transactions on Magnetics*, 51 (3): 1–4.
- Lipo, T. A.; W. Liu and Z. Du. (2020).** Comparison of AC motors to an ideal machine part II—non-sinusoidal AC machines. *IEEE Transactions on Industry Applications*, 56 (5): 4727–4737.
- Li, Y.; Z. Q. Zhu and G. J. Li. (2018).** Influence of stator topologies on average torque and torque ripple of fractional-slot SPM machines with fully closed slots. *IEEE Transactions on Industry Applications*, 54 (3): 2151–2164.
- Lu, Y.; J. Li; H. Xu; K. Yang; F. Xiong; R. Qu and J. Sun. (2021).** Comparative study on vibration behaviors of permanent magnet assisted synchronous reluctance machines with different rotor topologies. *IEEE Transactions on Industry Applications*, 57 (2), 1420–1428.
- Ni, Y.; X. Jiang; B. Xiao and Q. Wang. (2020).** Analytical modeling and optimization of dual-layer segmented halbach permanent-magnet machines. *IEEE Transactions on Magnetics*, 56 (5): 1–11.
- Raj, M. A. and Kavitha, A. (2017).** Effect of rotor geometry on peak and average torque of external-rotor synchronous reluctance motor in comparison with switched reluctance motor for low-speed direct-drive domestic application. *IEEE Transactions on Magnetics*, 53 (11): 1–8.
- User’s guide Maxwell-2D version15.0, Ansys, Inc. Electromagnetic Products. (2012).** Available online at: http://ansoft-maxwell.narod.ru/en/CompleteMaxwell2D_V15.pdf. Accessed on November 13, 2021.
- Vahaj, A. A.; A. Rahideh and T. Lubin. (2019).** General analytical magnetic model for partitioned-stator flux-reversal machines with four types of magnetization patterns. *IEEE Transactions on Magnetics*, 55 (11): 1–21.
- Wang, Y.; M. Filippini; G. Bacco and N. Bianchi. (2019).** Parametric design and optimization of magnetic gears with differential evolution method. *IEEE Transactions on Industry Applications*, 55 (4): 3445–3452.
- Xie, K.; D. Li; R. Qu; Z. Yu; Y. Gao and Y. Pan. (2019).** Analysis of a flux reversal machine with quasi-halbach magnets in stator slot opening. *IEEE Transactions on Industry Applications*, 55 (2): 1250–1260.
- Xu, F.; T. He; Z. Q. Zhu; Y. Wang; S. Cai; H. Bin; D. Wu; L. Gong and J. Chen. (2021).** Influence of slot number on electromagnetic performance of 2-pole high-speed permanent magnet motors with toroidal windings. *IEEE Transactions on Industry Applications*, 57 (6): 6023–6033.
- Zhang, H. S.; Z. X. Deng; M. L. Yang; Y. Zhang; J. Y. Tuo and J. Xu. (2020).** Analytical prediction of halbach array permanent magnet machines considering finite tooth permeability. *IEEE Transactions on Magnetics*, 56 (6): 1–10.
- Zhao, J.; X. Quan; X. Sun; M. Lin and S. Niu. (2020).** Influence of rotor-pole number on electromagnetic performance of novel double-rotor hybrid excited axial switched-flux permanent-magnet machines for EV/HEV applications. *IEEE Transactions on Magnetics*, 56 (3): 1–6.
- Zheng, M.; Z. Q. Zhu; S. Cai and S. S. Xue. (2019).** A novel modular stator hybrid-excited doubly salient synchronous machine with stator slot permanent magnets. *IEEE Transactions on Magnetics*, 55 (7): 1–9.
- Zhou, Y.; F. Fang and M. Zheng. (2019).** Research on fast design of key variables of bearingless flux-switching motor based on variable structure magnetic network. *IEEE Transactions on Industry Applications*, 55 (2): 1372–1381.
- Zhu, J.; L. Wu; W. Zheng; Q. Zhou and T. Li. (2021).** Magnetic circuit modeling of dual-armature flux-switching permanent magnet machine. *IEEE Transactions on Magnetics*, 57 (1): 1–13.